Supplementary Information (SI) for Journal of Materials Chemistry C.
This journal is © The Royal Society of Chemistry 2024

Electronic Supplementary Material (ESI)

Electronic Supplementary Information of Submission:

Unidirectional heat and fluid transfer performances of thermal diode with fishbone-microstructure wicks

Ping Li, Jiale Huang, Haifeng Qiu, Liangming Deng, Jiawei Liao, Tuo Jin, Yongfeng Zheng and Jianhua Xiang *

School of Mechanical and Electrical Engineering, Guangzhou University, Guangzhou, China

* ***E-mail****:* jhxiang@ gzhu.edu.cn

The Electronic Supplementary Information contains:

1 Simulation of unidirectional spreading on the fishbone structured surface
2 Experiment Section

Fig. S1 to Fig. S4
Table S1 Orthogonal experiment design of microstructure parameters of fishbone structure

Movie S1. Liquid flows unidirectionally on the fishbone microstructural surface
Movie S2. Water bidirectionally spreads in the gap of 0.5mm formed by two bare silicon chips without structures
Movie S3. Water unidirectionally spreads in the gap of 0.5mm formed by two fishbone structured silicon chips
Movie S4. A capillary rise with a height of 47 mm on the fishbone structured silicon chip with the forward arrangement
Movie S5. A capillary rise with a height of 14 mm on the fishbone structured silicon chip with the downward arrangement

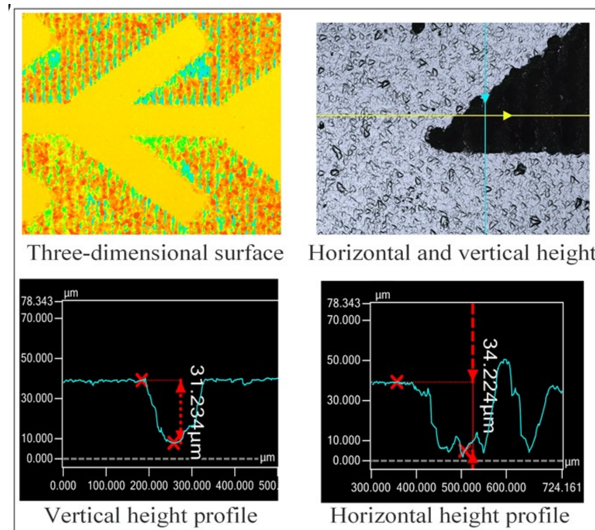

Fig. S1 The morphologies and profiles of the fishbone microstructured surface.

2 Simulation of unidirectional spreading on the fishbone structured surface

To preliminary discuss the effects of morphology parameters of fishbone structure on the unidirectional flow behavior, we carried out the simulation modelling by COMSOL Multiphysics based on the proposed theoretical analysis in Fig. S2. It is seen that the forward flow distance of the fluid on the fishbone structured surface is always greater than the reverse flow distance (Fig. S2a), resulting a typical unidirectional spreading. It is seen that the flow dipolarity can reach above 4.0 in the inclined angle α of 45°~60°. According to Eq.(6), the flow resistance ratio has a small value, which means that the forward flow suffers much less resistance than the reverse flow. When the inclined angle exceeds 65°, the fin of the fishbone is longer, resulting in a smaller gap width between two inclined fins and relatively smaller flow. This can also be proved by Fig. S2b that both forward flow distance and flow dipolarity are all reduced as the gap width is less than 0.8 mm. Hence, it is more conducive to the forward flow for the inclined angle lies between 50° and 55°.

Fig. S2b shows the influence of gap width between fishbone fins on flowing performance. The flow dipolarity showed a trend of first rising and then decreasing, and the maximum flow dipolarity of 4.25 occurred at 0.8 mm. Even though the forward flow distance increases with the increase of the gap width, the reverse flow distance increases when the spacing exceeds 0.8 mm. This may be because the asymmetric resistance of the fishbone structure decreases with the increase of the spacing (Eq.(7)), and the difference between the forward and reverse flow resistance of the fluid also decreases (Eq.(6)). Thus, a more obvious unidirectional flow is seen at a relatively narrow gap width. However, if the

spacing is too small, it will increase the possibility of forming a closed area and hindering the flow on the one hand; on the other hand, it will short the inclined fin length and fail the structural resistance. Therefore, the gap width of d=0.8 mm shows a greater flow dipolarity.

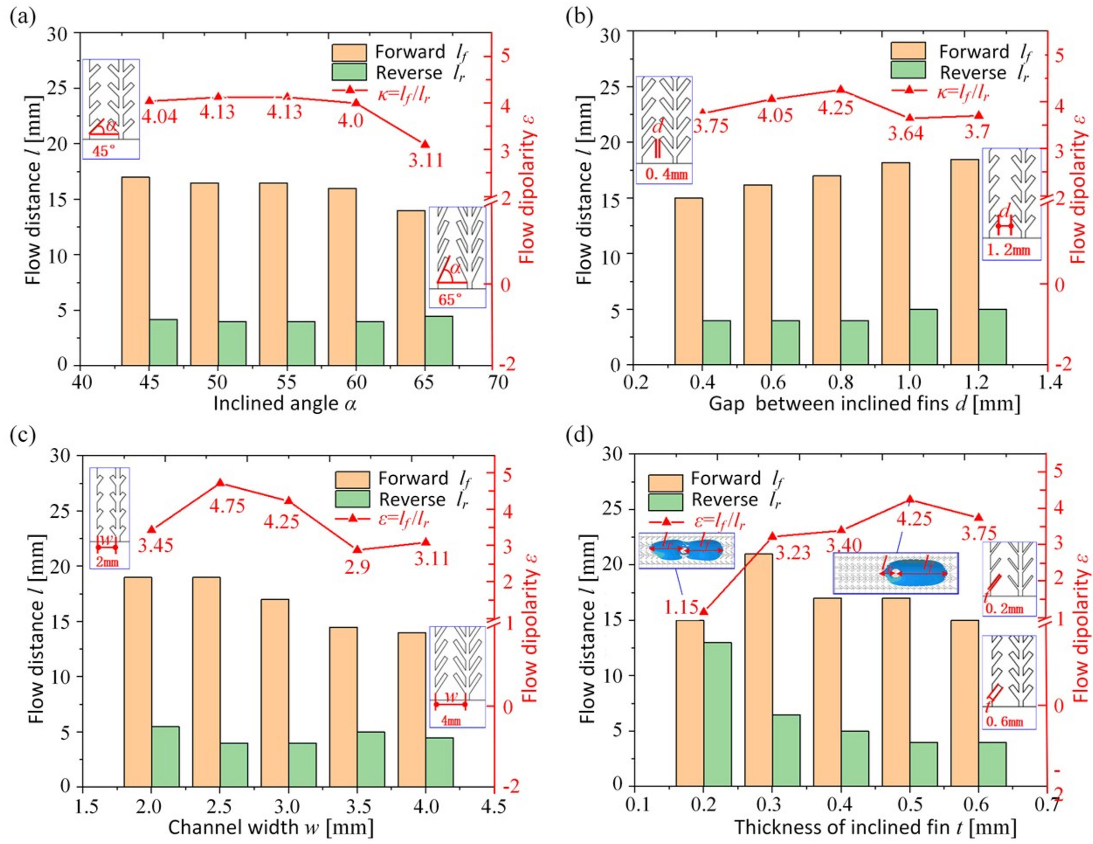

Fig. S2 Relationship between liquid unidirectional fluidity and structural parameters of fishbone structures: (a) inclined angle, (b) inclined fin gap, (c) channel width and (d) inclined fin thickness.

The flow conditions on the fishbone structured surface with different channel widths are shown in Fig. S2c. The fishbone structured surfaces with the channel widths of w=2.5 mm and w=3 mm have a larger flow dipolarity, which is 4.75 and 4.25, respectively. This is because the forward flow distance is longer and the reverse flow distance is shorter in these two surfaces. This case can be attributed to: firstly, a narrower channel produces a shorter inclined fin, resulting a decrease in structural resistance. Conversely, a wider channel resulted a greater flow resistance, decreasing the forward flow distance. Thirdly, a wider channel width requires more liquid to support a continuous flow. Based on two-phase (vapor and liquid) heat transfer in a confined space, the internal chamber of thermal diodes needs a suitable space for mass and heat transport and appropriate amount of working fluid. Therefore, it is necessary to choose a suitable range of channel width.

Fig. S2d shows the flow on the fishbone structured surface with different inclined fin thicknesses.

The flow dipolarity decreases as the inclined fin is thinner. It exhibits a unidirectional flow until the inclined fin decrease to 0.2 mm. At this point, the value of flow dipolarity is almost 1.0 (l_f and l_r are 15 mm and 13 mm, respectively). This is because the reduce of inclined fin thicknesses will lower the microstructural resistance and flow resistance for both forward flow and reverse flow. However, increase the thickness of inclined fin will lead to the increase of the flow resistance, the flow distance is then decreased. It is seen that the maximum flow dipolarity of 4.25 appears at the inclined fin thickness of t=0.5 mm, which shows a good unidirectional effect.

Based on the above simulation results, it is not difficult to draw the conclusions that, for a greater flow dipolarity, the inclined angle α should lie between 50°~55°, the channel width w is chosen about 2.5~3 mm, the gap width and the inclined fin thickness should be selected around d =0.8 mm and t = 0.5 mm, respectively.

2 Experiment Section

Structural design and encapsulation of thermal diode: To test the heat transfer performance, we encapsulate the fishbone microstructured silicon chips as wicks in a flat copper tube to be a thermal diode. It is divided into upper and lower parts, as shown in Fig. S3a. The upper and lower shells are made of copper and polycarbonate (PC). The upper shell is a copper plate with a platform on the inner surface. The lower shell is a sunken part with a large inclined plane at condenser chamber and two small inclined planes on both sides. The left and right sides of the copper shell and PC structure are bonded together by using the binder (with a mixing ratio of 1:1 of epoxy: hardener). Two fishbone microstructured silicon wafers are face-to-face with a gap of 0.5 mm fixed to the middle position between the bottom and top shells as wicks to provide sufficient capillary pressure. Then, two chambers are formed: evaporator chamber and condensing chamber. To storage the working fluid as well as increase the boiling efficiency, a hydrophilic copper mesh is placed on evaporator chamber and fixed by pressing plate and part of it was inserted into the wick. A copper tube was connected to the evaporator chamber by a connector. Then, encapsulated the thermal diode and injected the deionized water into it via the filling tube. The filling ratio is defined as the volume ratio of the working fluid (deionized water) to the whole internal space of the thermal diode. Finally, evacuated the air in the thermal diode and sealed the filling tube by stamping. Key dimensions of the thermal diode are shown in Fig. S3b. The total thickness of the encapsulated thermal diode is 3.5 mm, the total length is 141 mm,

and the total width is 36 mm. A narrow flat cavity is used as fluid channel, while two large grooves with triangle cross-sectional shape are served as gas channel. Three inclined surfaces on the bottom shell are linked to the fluid channel, which can guide the condensed liquid to flow into the microstructure channel. The morphologies and profiles of the microstructured silicon wafer are shown in Fig. S1.

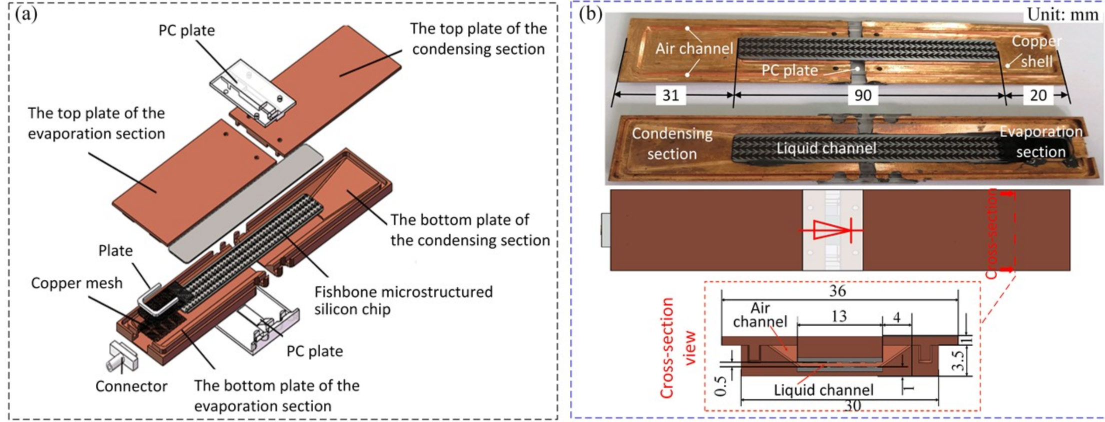

Fig. S3 Thermal diode with the fishbone microstructured wick. (a) Structural composition and (b) internal diagram of thermal diode.

Experimental setup and data calculation of temperature: The experimental setup consists of four modules, including heating module, water-cooling module(water bath tank), rotating platform(rotation angle of -90º~90º)，DC power source and data acquisition unit, as shown in Fig. S4a. The total heating power can be adjusted by the DC power source. The heating module, the cooling module, the thermocouples and the thermal diode are placed on the rotating platform (Fig. S4b). The heating block and the adiabatic section of thermal diode are wrapped by the insulation materials to minimize the heat loss and enhance the test accuracy. Temperature data at different locations were collected by thermocouples and transferred to the computer by acquisition unit. Temperature data at different locations, here are T_1-T_4 four temperatures (Fig. S4c), were collected by thermocouples and transferred to the computer by acquisition unit. Heat generated from the heat source is transferred from the evaporating section to the condensing section, and finally carried away through the water-cooling module.

The thermal performance of thermal diode can be estimated by thermal resistance as follows

$$R = \frac{T_e - T_c}{P} \tag{1}$$

Where T_e and T_c are the average temperature of evaporator ad condenser, respectively. P is the heating power, which can be directly acquired from DC power source. T_e and T_c are calculated as follows.

$$T_e = \frac{T_1 + T_2}{2} \tag{2}$$

$$T_c = \frac{T_3 + T_4}{2} \tag{3}$$

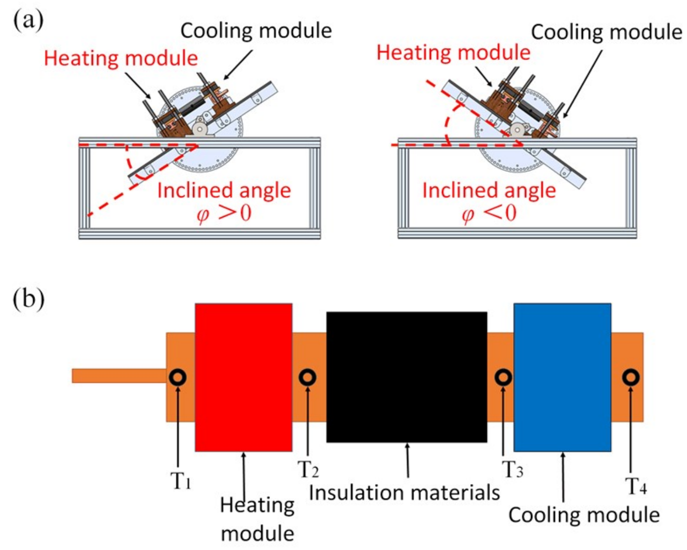

Fig. S4 Schematic diagram of (a) rotating platform and (b) position of thermocouple.

Table S1 Orthogonal experiment design of microstructure parameters of fishbone structure

No.	Inclined angle α °	Gap d (mm)	Fin thickness t (mm)	Structural resistance ratio χ	Flow resistance ratio f	Resistance ratio ($x+\eta$)	Flow dipolarity ε	Capillary rise height Lc (mm)	Thermal resistance R	Thermal dipolarity κ
1	50	0.6	0.4	4.24	2.49	6.73	6.5	14.5	2.09	1.22
2	**50**	**0.8**	**0.5**	**3.13**	**1.84**	**4.97**	**21.0**	**41.0**	**0.63**	**3.43**
3	50	1	0.6	2.39	1.40	3.80	8.7	22.0	1.92	1.27
4	55	0.6	0.5	3.17	2.13	5.30	13.5	36.0	0.89	2.46
5	55	0.8	0.6	2.44	1.64	4.08	9.3	27.5	1.71	1.36
6	55	1	0.4	3.36	2.25	5.61	10.6	29.0	1.08	1.46
7	60	0.6	0.6	2.50	1.88	4.38	12.0	30.5	1.02	1.49
8	60	0.8	0.4	3.46	2.60	6.06	8.8	25.0	1.81	1.33
9	60	1	0.5	2.54	1.91	4.45	12.5	34.5	0.96	2.04
10*	52.5	0.8	0.5	3.03	1.90	4.93	21.0	46	0.42	4.05
11*	55	0.8	0.5	2.93	1.97	4.90	18.5	39.5	0.83	2.95
12*	Bare silicon			0	0	0	1	5	2.91	1.06
13*	Copper shell			0	0	0	1	0	4.28	0.98